

Minghua Zhang¹, Shuaiqi Tang^{1,2}, Shaocheng Xie²
¹Stony Brook University, State University of New York
²Lawrence Livermore National Laboratory

1. Background

Cloud resolving models (CRM), Large-Eddy Simulation (LES) and single-column models need vertical velocity and advective tendencies of temperature and water as input to simulate clouds, radiation and other related fields.

ARM/GCSSS conducted a case study of simulating clouds by using SCMs and CRMs for a frontal passage over the ARM SGP during the March 2000 Cloud IOP (Xie et al. 2005). The large-scale vertical velocity and advective tendencies over a domain of about 300 km in diameter centered at the SGP CF are used as forcing data. They are shown in Figure 1.1. The time-pressure cross sections of the observed and simulated cloud amount by CRMs and SCMs are shown in Figure 1.2.

In addition to model errors, the ARM/GCSSS Case Study concluded that the model-observation differences are partially due to the coarse resolution of the specified forcing data as can be inferred from Figure 1.3. The purpose of this study is to improve the specifications of the dynamics.

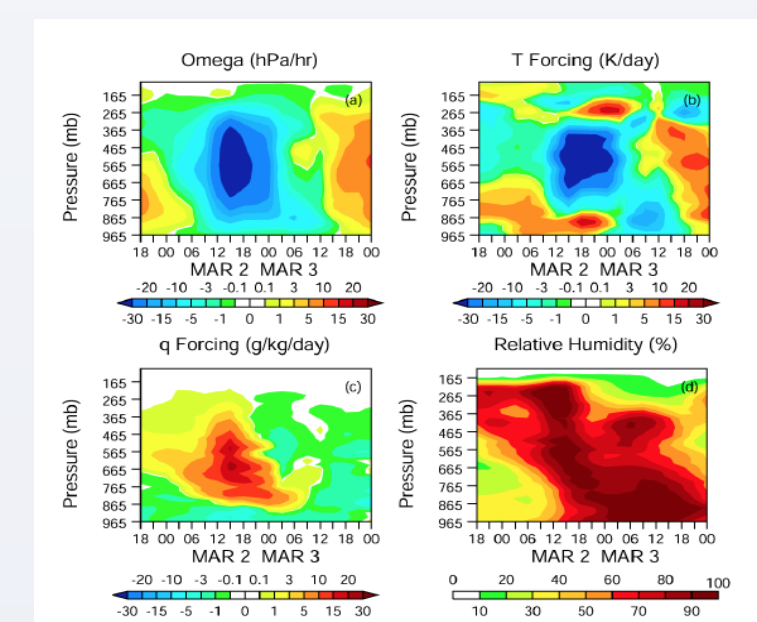


Figure 1.1. The time-pressure cross sections of the domain-averaged (a) vertical velocity (hPa hr⁻¹), (b) total temperature advection (K day⁻¹), (c) total moisture advection (g kg⁻¹ day⁻¹), and RH (%), for the ARM/GCSSS frontal case study in March 2000 over the SGP.

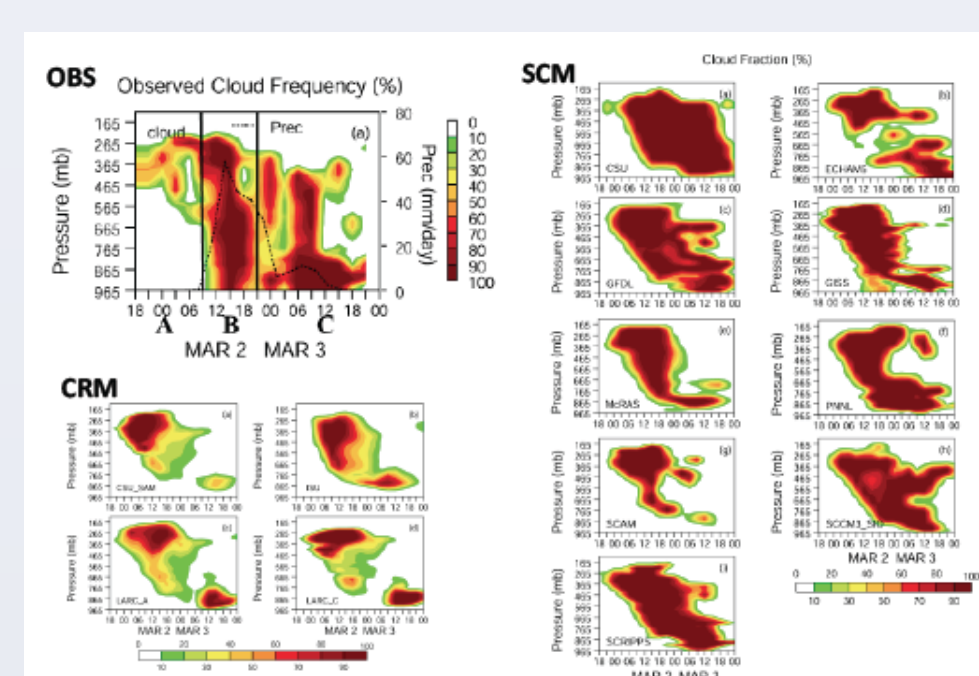


Figure 1.2. The time-pressure cross sections of the CRM-produced and SCM produced cloud fractions (%) for the frontal case.

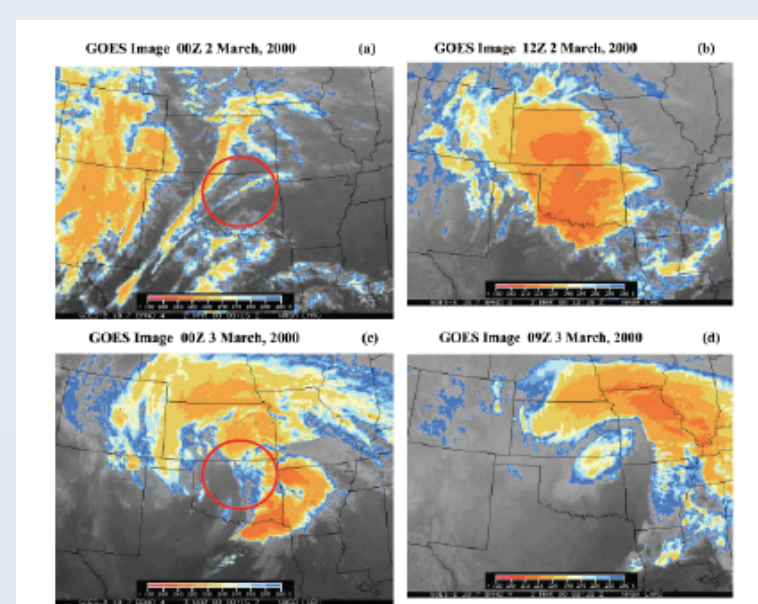


Figure 1.3. The GOES cloud image at (a) 00Z 2 March, (b) 12Z 2 March, (c) 00Z 3 March, and (d) 09Z 3 March, 2000.

2. A Three-Dimensional Constrained Variational Analysis Algorithm (3DCVAR)

Building on the constrained variational analysis algorithm of atmospheric vertical velocity and advective tendencies for a single column of Zhang et al. (2001), we developed the 3DCVAR. The algorithm uses pre-processed 0.5°x0.5° resolution gridded data of precipitation, surface turbulent heat fluxes, and radiative fluxes at TOA and surface as input to constrain the initial guess fields from operational analysis and reanalyses (Figure 2.1 and 2.2).

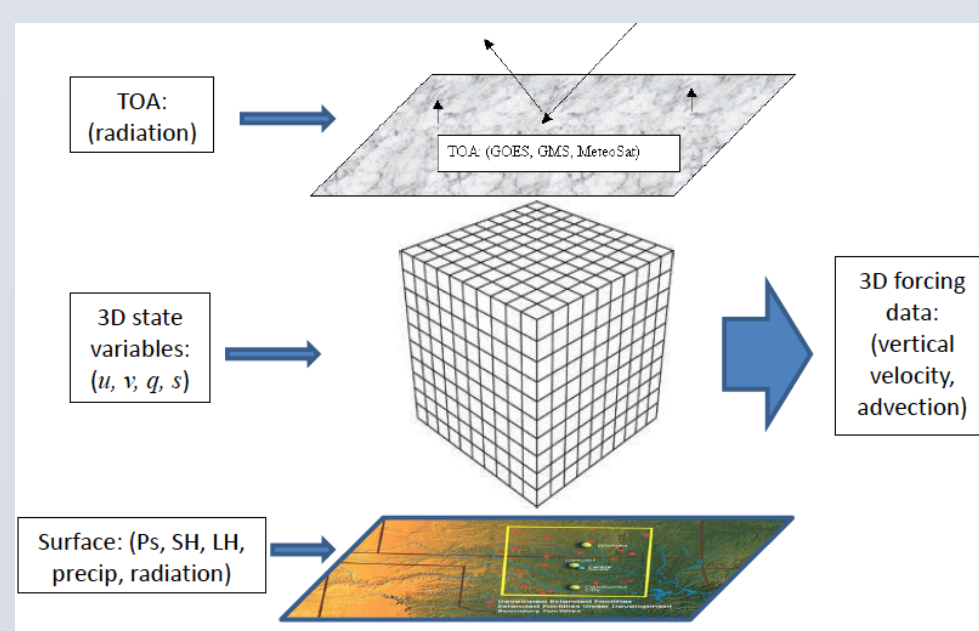


Figure 2.1: schematic figure of the 3DCVA. It shows the inputs of background data (3D state variables), surface and TOA constraint variables, and the output of 3D large-scale forcing data.

$$J = \int_{\Omega} \left[\frac{1}{2} \int_{p_0}^{p_1} \left(\frac{\partial \omega}{\partial t} - \nabla \cdot \mathbf{v} \right)^2 + \frac{1}{2} \int_{p_0}^{p_1} \left(\frac{\partial T}{\partial t} + \nabla \cdot \mathbf{v} T + \frac{\partial q}{\partial t} + \nabla \cdot \mathbf{v} q \right)^2 \right] d\Omega$$

$$\mathcal{L} = \int_{\Omega} \left[\frac{1}{2} \int_{p_0}^{p_1} \left(\frac{\partial \omega}{\partial t} - \nabla \cdot \mathbf{v} \right)^2 + \frac{1}{2} \int_{p_0}^{p_1} \left(\frac{\partial T}{\partial t} + \nabla \cdot \mathbf{v} T + \frac{\partial q}{\partial t} + \nabla \cdot \mathbf{v} q \right)^2 \right] d\Omega$$

$$J(X) = \int_{\Omega} \left[\frac{1}{2} \int_{p_0}^{p_1} \left(\frac{\partial \omega}{\partial t} - \nabla \cdot \mathbf{v} \right)^2 + \frac{1}{2} \int_{p_0}^{p_1} \left(\frac{\partial T}{\partial t} + \nabla \cdot \mathbf{v} T + \frac{\partial q}{\partial t} + \nabla \cdot \mathbf{v} q \right)^2 \right] d\Omega$$

Figure 2.2: the adjusted C-grid used in 3DCVA. All the constraint variables (precipitation, radiation, surface fluxes) are at the grid center and represent grid average. Red arrows show the correlation of the center variable to its surrounding variables.

In the 3DCVA algorithm, all atmospheric columns satisfy conservations of atmospheric mass, energy and total water simultaneously. Precipitation in a grid box can remotely constrain the accuracy of advective transport and vertical velocity in other grid boxes.

The product can serve three purposes:

- 1) It provides modeling forcing at higher spatial resolution
- 2) It allows the SCM/CRM/LES to be placed where there are clouds
- 3) It contains 3-D fields of apparent heating (Q1) and moisture sinks (Q2)

Tang, S., and M. Zhang (2015), Three-dimensional constrained variational analysis: Approach and application to analysis of atmospheric diabatic heating and derivative fields during an ARM SGP intensive observational period, *Journal of Geophysical Research: Atmospheres*, 120(15), 7283-7299, doi: 10.1002/2015JD023621.

Xie, S., et al. (2005), Simulations of midlatitude frontal clouds by single-column and cloud-resolving models during the Atmospheric Radiation Measurement March 2000 cloud intensive operational period, *Journal of Geophysical Research: Atmospheres*, 110(D15), D15503, doi: 10.1029/2004JD005119.

Zhang, M., J. Lin, R. T. Cederwall, J. J. Yio, and S. C. Xie (2001), Objective Analysis of ARM IOP Data: Method and Sensitivity, *Monthly Weather Review*, 129(2), 295-311, doi: 10.1175/1520-0493(2001)129<0295:OAOAID>2.0.CO;2.

3. The March 3rd, 2000 Frontal System and 3DVAR Analysis

The synoptic meteorology associated with the frontal system in the ARM/GCSSS Case Study is captured by analysis/reanalysis products (contours in Figure 3.1 and 3.2). However, in the smaller domain of about 300 km x 300 km (red boxes), the moisture field and vertical velocity field differ greatly from each other.

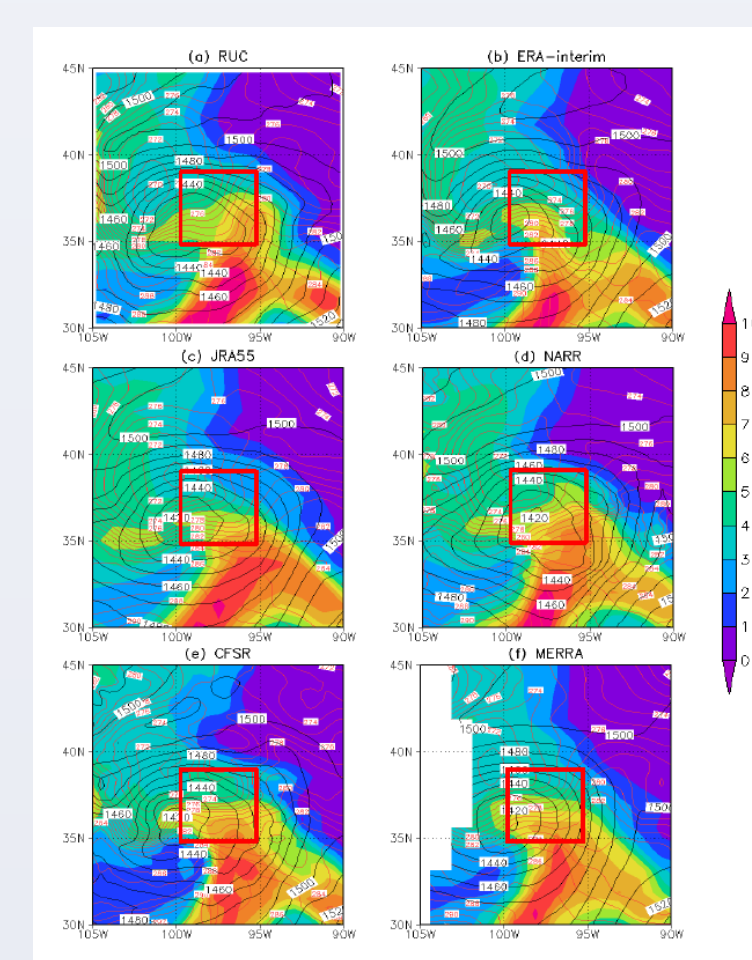


Figure 3.1: 850hPa Geopotential height (gpm, black lines), temperature (K, red lines) and specific humidity (g kg⁻¹, shaded) from (a) RUC, (b) ERA-Interim, (c) JRA 55, (d) NARR, (e) CFSR, (f) MERRA at 00Z Mar 3rd 2000. The red box indicates the SGP domain.

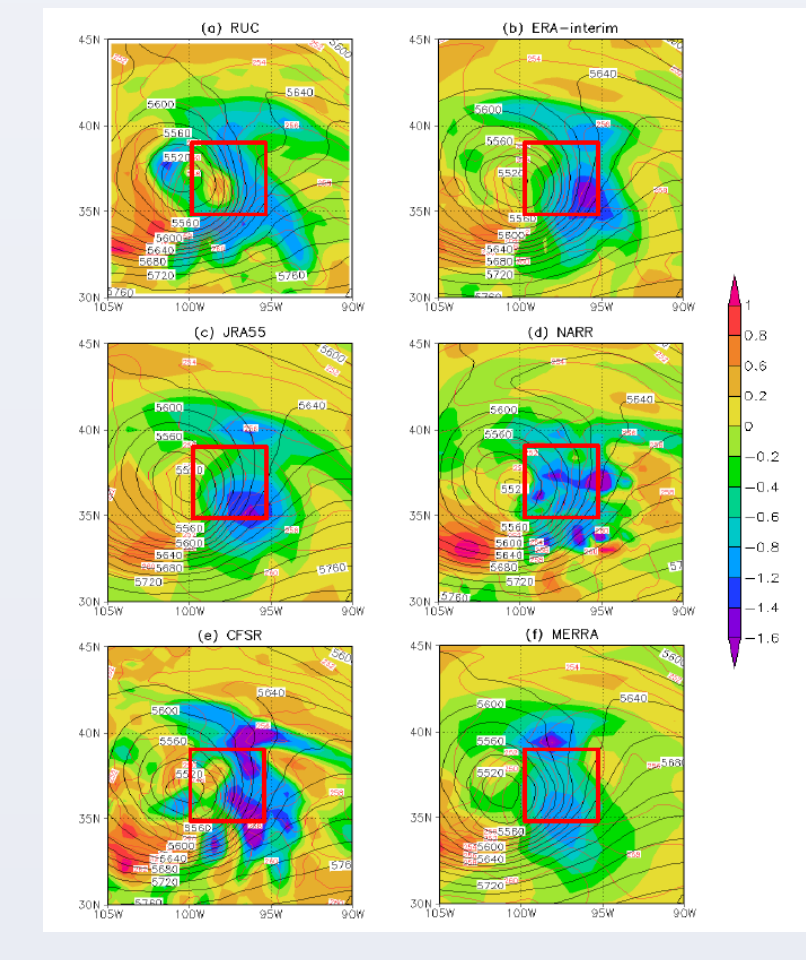


Figure 3.2: Same as Figure 4.2 except that the shading is for vertical velocity (Pa s⁻¹) and the level is 500hPa.

The reliability of the analysis/reanalysis products in capturing the vertical velocity and advective tendencies within the SGP domain can be evaluated by using the vertically integrated Q1 field shown in Figure 3.3 since this can be compared with precipitation observations (Figure 3.4b). The analysis/reanalysis products have large biases in the spatial distribution. The corresponding field in 3DCVA (Figure 3.5) is consistent with precipitation observations. The 3DVA also provides the Q1 and Q2 fields coupled within the frontal circulation system that are physical consistent with other observations (Figure 3.6).

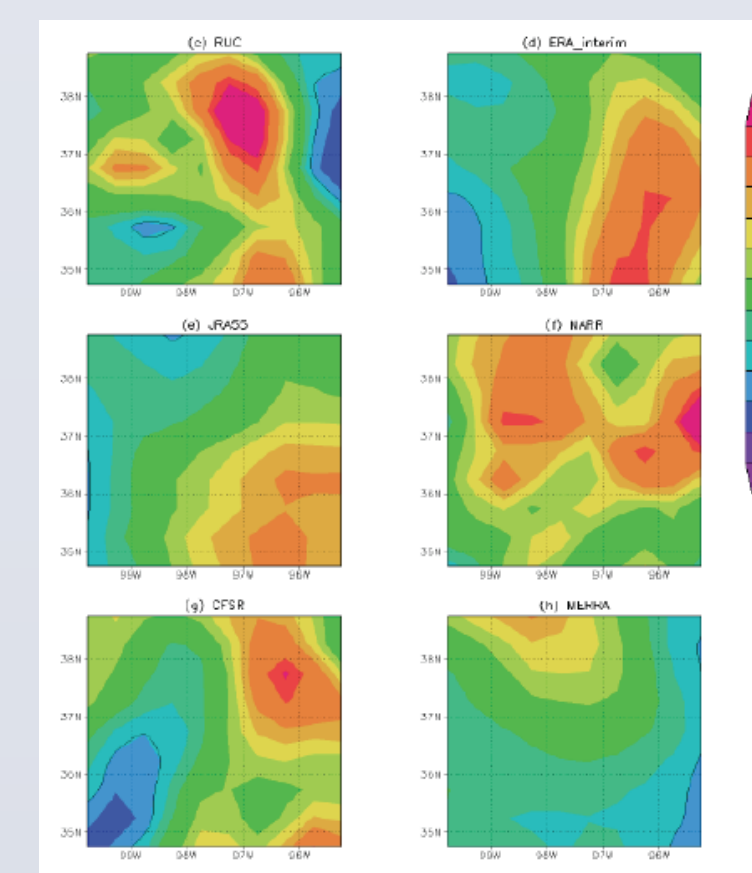


Figure 3.3. The vertically integrated Q1 from RUC, ERA Interim, JRA 55, NARR, CFSR and MERRA at 00Z Mar 3 2000. The unit is mm/day.

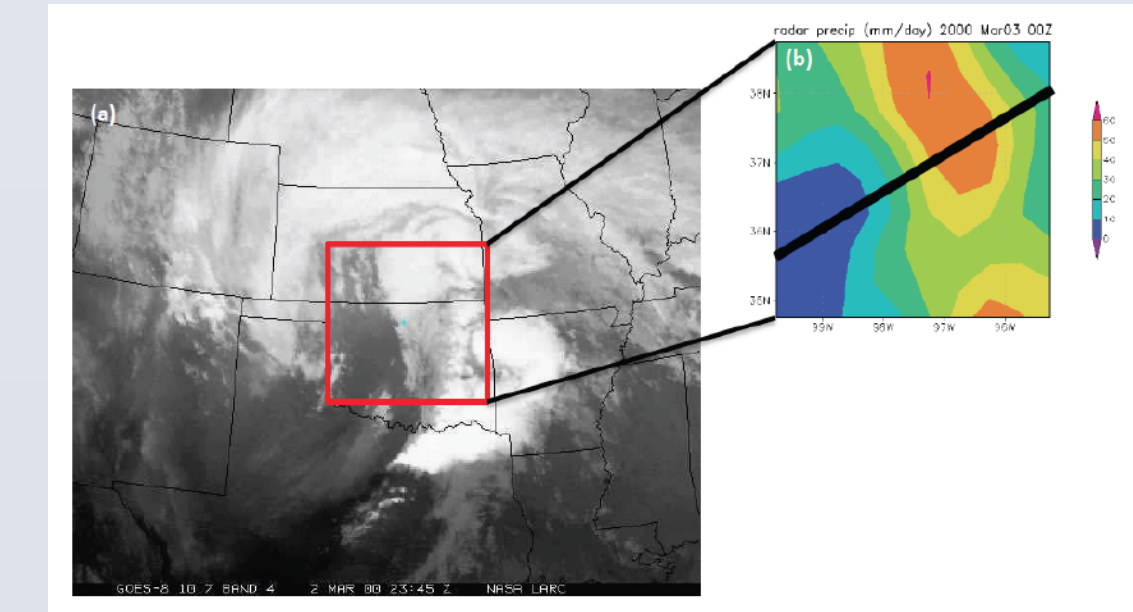


Figure 3.4. (a) GOES-8 satellite cloud image at 23:45Z March 2nd 2000. The red box shows the SGP domain applying 3DCVA. (b) 3-hourly precipitation rate centered at 00Z Mar 3rd averaged into 0.5°x0.5° horizontal resolution from the Arkansas-Red Basin River Forecast Center (ABRFQ). The bold black line shows the position of cross-front section in later figures.

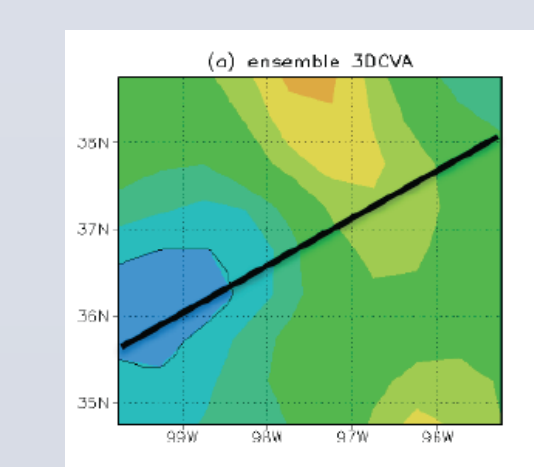


Figure 3.5. The vertically integrated Q1 from 3D Variational Analysis and from the ensemble mean first-guess fields.

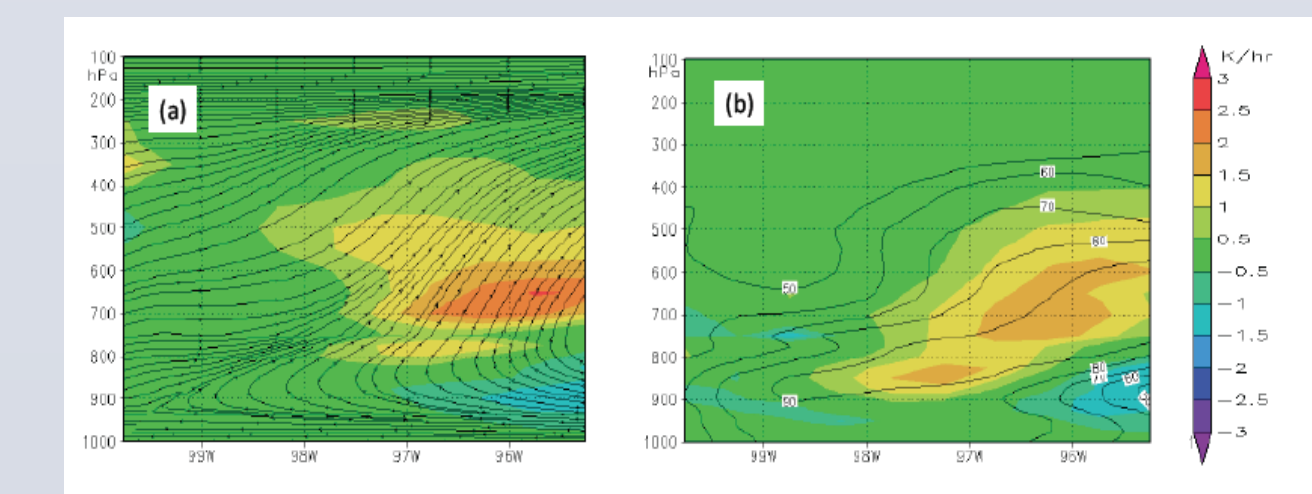


Figure 3.6: cross section of analyzed 3DCVA fields along the cross section in Figure 3.4. (a) Q1 (color) and circulation along the cross section (streamlines); (b) Q2 (color) and relative humidity (contour)

4. Summary

- 1) We have developed the 3DCVA algorithm to derive atmospheric vertical velocity and advective tendencies at 0.5°x0.5° spatial resolution over the ARM SGP. The gridded fields are physically consistent with the spatial distribution of surface measurements of precipitation, radiation and turbulent heat fluxes.
- 2) A 3DCVA dataset at 0.5°x0.5° spatial resolution has been produced for the March 2000 ARM SGP IOP. The data can be used to force SCM/CRM/LES targeting different clouds within the SGP domain. It can also be used to describe the coupling of the diabatic heating (Q1) and moisture sinks (Q2) with circulation fields.